Article

Effect of Laser Surface Structuring on Surface Wettability and Tribological Performance of Bulk Metallic Glass

Qinghua Wang [1] , Yongqi Zhou [1], Pengyu Wu [1], Chengyu Qu [1] and Huixin Wang [2],*

1 Jiangsu Key Laboratory for Design and Manufacture of Micro-Nano Biomedical Instruments, School of Mechanical Engineering, Southeast University, Nanjing 211189, China; qinghua-wang@seu.edu.cn (Q.W.); 213192271@seu.edu.cn (Y.Z.); 213193135@seu.edu.cn (P.W.); 213192415@seu.edu.cn (C.Q.)
2 Institute of Agricultural Facilities and Equipment, Jiangsu Academy of Agricultural Sciences, Nanjing 210014, China
* Correspondence: wanghx17@mails.jlu.edu.cn; Tel.: +86-1-894-033-1946

Abstract: Bulk metallic glasses (BMGs) have been extremely popular in recent decades, owing to their superior properties. However, how to improve the surface functions and durability of BMGs has always been a key engineering issue. In this work, a facile laser-based surface structuring technique was developed for modulation and control of the surface functionalities of Zr-based BMG. For this technique, a laser beam was first irradiated on the surface to create periodic surface structure, followed by heat treatment to control surface chemistry. Through experimental analyses, it was clearly shown that laser surface structuring turned the BMG surface superhydrophilic, and subsequent heat treatment turned the surface superhydrophobic. We confirmed that the combination of laser-induced periodic surface structure and modified surface chemistry contributed to the wettability transition. The laser-heat-treated surface also exhibited improved antifriction performance with the help of lubrication medium. This work provides a feasible method for surface modification of BMG, suggesting applications in the areas of medicine, biology and microelectronics.

Keywords: laser surface structuring; metallic glass; surface morphology; surface chemistry; wettability; tribological performance

1. Introduction

In contrast to traditional crystalline materials, bulk metallic glasses (BMGs) are a class of metallic materials without long-range translational order [1,2]. This unique material structure endows BMGs with superior mechanical and physical properties, including ultrahigh strength and hardness [3,4], good corrosion and wear resistance [5], etc. These properties make BMGs suitable for a series of key applications in the areas of mechanical engineering, materials engineering, microelectronics and biomedical devices [6,7]. Consequently, development of forming and processing techniques for BMGs has become a popular research topic, triggering the emergence of various techniques, including copper mold casting [8], nanomolding [9–11], magnetron sputtering [12,13] and microarc oxidation [14]. However, with increasing demand for fabrication of complex BMG components, the abovementioned techniques present significant limitations. For example, the processing efficiency of the copper mold casting process is relatively satisfactory, although it also imposes limitations on the forming size of BMG components. In addition, although the forming accuracy of nanomolding techniques is very high, they also limit the forming size of BMG components, in addition to high requirements for powder constituents. Other techniques, such as conventional machining [15] and microelectro-discharge machining [16], tend to crystallize the BMG materials during the machining process.

Therefore, development of high-efficiency processing techniques for BMGs is of great significance. In recent years, laser surface texturing has been demonstrated as an efficient method for processing metallic materials [17–25] due to several key advantages, such

as high precision, high process flexibility, ease of automation and low environmental pollution. When processing BMGs using pulsed lasers, the heating and cooling cycles can be well controlled; thus, BMGs can be manufactured without the tendency of being crystallized. Some research progress has been achieved in the area of pulsed laser texturing for BMGs. Huang et al. [26] fabricated hierarchical micro/nanostructures on Zr-based BMG using nanosecond pulsed laser texturing. The experimental results demonstrated that the effective surface area on BMG was increased via laser texturing, and the material retained an amorphous state and exhibited uniformly distributed surface chemistry. Jiao et al. [27] fabricated periodic surface structures, including microdimples and microgrooves on Zr-based BMG using nanosecond-based laser texturing. The surface characterization results indicated that the wettability [28] and biocompatibility [29] of BMG is strongly correlated with its laser-induced surface structure and chemistry. Du et al. [30] created four different types of laser-induced periodic surface structures on Zr-based BMG using a femtosecond laser. The experimental results demonstrated that laser-induced surface structures can effectively reduce the adhesion of bacteria on BMG substrates, improving the antibacterial properties of BMG. This indicates that pulsed laser texturing has become an important method for fabrication and manufacturing of BMGs, particularly in the area of surface modification and functionalization.

Owing to the high hardness of BMGs, they have been considered promising candidates for high-wear applications. However, to realize industrial applications, researchers are still exploring high-efficiency and low-cost methods to enhance the tribological properties of BMG. Sawyer et al. [31] utilized ceramic conversion treatment to convert the surface of BMG into ceramic layers, which significantly improved the tribological properties of the BMG. Wu et al. [32] investigated the effect of oxygen on the tribological behavior of a Zr-based BMG using pin-on-disk wear test. The experimental results indicated that the wear rate of BMG was substantially increased with the increase in oxygen content, demonstrating the importance of environmental condition for determining the tribological performance of BMG. Wu et al. [33,34] also prepared Ti-based metallic glass composite coatings by laser cladding and investigated the tribological behavior of both the substrate and coatings. The experimental results indicated that with the addition of Sn, both the hardness and wear resistance of the laser-cladded coatings can be significantly improved. This reveals that with a proper surface treatment technique, the tribological performance of BMG can be considerably improved.

Nevertheless, although laser texturing has been demonstrated as a high-efficiency method for processing BMGs, some issues still remain. On the one hand, although researchers have modified the surface functionalities of BMGs by laser texturing, control and tuning of the related functionalities, such as how to realize switchable control of surface wettability from superhydrophilicity to superhydrophobicity, remains a challenge. On the other hand, little research progress has been achieved with respect to improving the tribological performance of BMGs using laser-based methods, and further exploration is urgently needed in this area.

In this work, a laser-based surface structuring technique was developed to functionalize the BMG surface. The technique mainly consists of two steps: first, a nanosecond pulsed laser was utilized to induce the generation of a periodic surface structure on the BMG surface; then, heat treatment was employed on laser-structured BMG surface to modify the surface chemistry. Furthermore, the surface structure, surface chemistry, surface wettability and tribological performance of the BMG surfaces with different treatment steps were characterized. The experimental results indicated that with the combined effects of laser surface structuring and heat treatment, a periodic surface structure was generated on the BMG surface, and the surface wettability was converted from superhydrophilicity to superhydrophobicity. In the meantime, with the help of lubrication medium, the laser-heat-treated superhydrophobic BMG surface exhibited significantly improved tribological performance. The developed technique provides a reliable method for processing BMG, with strong potential for applications in diverse areas.

2. Materials and Methods

2.1. Materials

Commercially available Zr-based bulk metallic glass (BMG) Vitreloy 1 (purchased from METALLAB, Changzhou, China) was used in this work. The samples were first machined into thin sheets with dimensions of 30 mm × 30 mm × 2 mm and then mechanically grinded. Before the laser surface structuring experiments, the samples were ultrasonically cleaned successively with acetone, ethanol and deionized water.

2.2. Laser Surface Structuring

In this work, laser surface structuring experiments were conducted with a laser marking machine (TH-UV200A, Tianhong Laser, Suzhou, China) equipped with a 355 nm UV laser source (AWAVE 355-15W-30K, Advanced Optowave Corporation, Ronkonkoma, NY, USA). The laser beam is emitted by the laser source and guided by reflective mirrors. The attenuator and beam expander control the intensity and laser beam diameter, respectively. The focal spot diameter provided by the focusing lens of the system was ~35 μm in this work. A unidirectional line pattern was used for surface fabrication, as shown in Figure 1. The laser processing parameters can be found in Table 1, and schematics of the laser surface structuring and heat treatment experiments are shown in Figure 2.
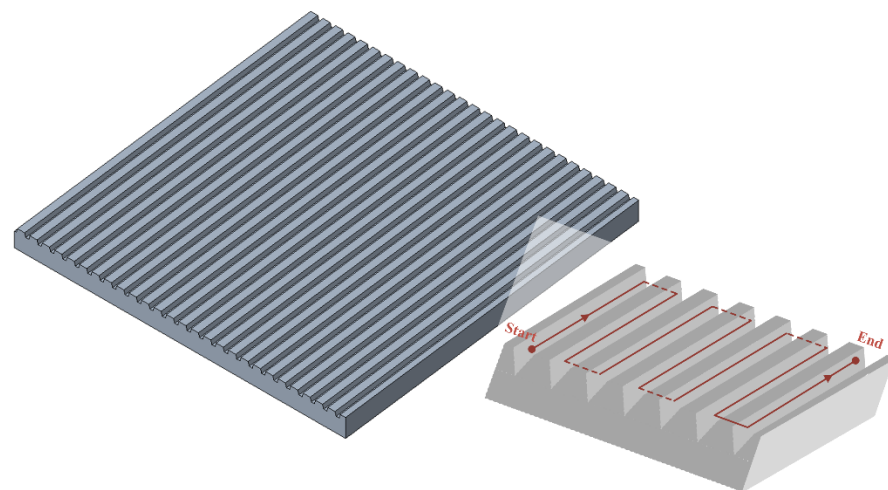

Figure 1. Pattern design used for laser surface structuring of BMG.

Table 1. Processing parameters for the laser-based surface structuring experiments.

Name of Parameter	Value
Average power (W)	15.0
Repetition rate (kHz)	30
Pulse width (ns)	20
Scanning speed (mm/s)	20, 40, 60, 80
Step size (μm)	150
Power intensity (GW/cm^2)	2.60
Pulse energy (mJ)	0.5
Heat treatment temperature (°C)	150
Maximum heat treatment duration (hours)	2

Immediately after laser surface structuring, the laser-structured BMG surfaces became superhydrophilic. With low-temperature annealing treatment in a conventional furnace, the laser structured BMG surfaces achieved wettability transition. During the heat treatment, the annealing temperature was set to 150 °C, and the treatment duration was set to a maximum of 2 h.
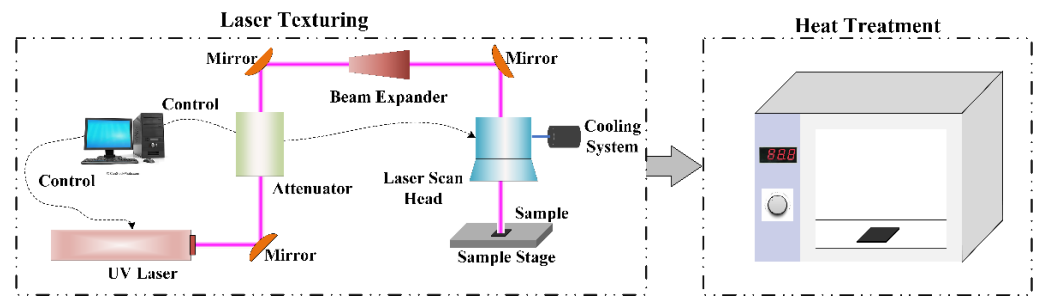
Figure 2. Schematic of the laser-based surface structuring experiments of BMG.

2.3. Surface Characterizations

The surface morphology was analyzed using a field emission scanning electron microscope (FESEM, FEI Sirion, Hillsboro, OR, USA), and the surface chemistry was analyzed using energy-dispersive X-ray spectroscopy (EDX, FEI Sirion, Hillsboro, OR, USA) and X-ray photoelectron spectroscopy (XPS, PREVAC, Rogów, Poland). For the surface wettability, water contact angle (WCA) measurements were performed using a contact angle goniometer (SDC-200, Sindin Precision Instrument Co., Ltd., Dongguan, China). For each measurement, a water droplet with a volume of ~4 μL was dropped onto the sample surface. A CMOS camera was used to capture an optical image of the water droplet, and image analysis software was employed for WCA value analysis. For experimental accuracy, four WCA measurements were performed for each sample, and the average value was reported with the standard deviation.

Wear resistance was evaluated using a ball-on-disc wear tester (WTM-2E, Zhongkekaihua Technology Development Co., Ltd., Lanzhou, China). The pin was a Si_3N_4 ceramic ball with a 4 mm diameter, and the sample surface was used as the disk. The wear test was conducted under a load of 4 N and a rotational speed of 150 rpm, and the test duration was set to 10 min. Before the test, the surface was pre-rubbed for 2 min to ensure full contact of the friction pairs.

3. Results

3.1. Surface Morphology

The SEM micrographs of the untreated BMG surface and laser-structured BMG surfaces at different scanning speeds can be found in Figure 3. As seen in Figure 3a, the untreated BMG surface shows high flatness and low surface roughness, and only some horizontal grinding marks are visible on the surface. However, after laser surface structuring, the laser-structured surfaces exhibit highly distinct surface morphology, as shown in Figure 3b–e. With relatively low scanning speed (20 mm/s, Figure 3b), the laser-structured surface exhibits a periodically arrayed linear bump structure at the micron level with a step size of 150 μm. Between microbump paths, some tiny submicron and nanoscale particles can be observed, which could be attributed to the strong ablation and evaporation of the substrate material during laser–material interaction, resulting in the redeposition of these particles on the surface. As the scanning speed increases (40 mm/s, Figure 3c), the microbump structure is still present on the surface, whereas the structural uniformity slightly decreases. When the scanning speed is further increased to 60 mm/s (Figure 3d) and 80 mm/s (Figure 3e), the surface morphology of the laser-structured surfaces exhibits distinct transformation from microbump structure to microconcave structure. In the meantime, it is clearly observed that some micro-/nanoscale particles are distributed on the laser-scanned path, regardless changes in scanning speed. The experimental results indicate that the surface structure can be effectively modulated by controlling the laser processing parameters. Figure 4 shows the surface morphology of the laser-structured BMG surfaces at different scanning speeds before and after heat treatment. It can be clearly observed that the surface morphology of different surfaces remains almost unchanged after heat treatment, indicating that heat treatment does not affect the surface morphology. For the variation

of surface structures subject to different laser processing conditions, Huang et al. [35] processed Zr-based metallic glass with varied laser processing parameters using a 1064 nm nanosecond laser and observed the transformation from microconvex structure to microconcave structure on the laser-textured surface. The authors proposed that the structural transformation could be ascribed to the combined effects of recoil pressure and Marangoni flow during laser–material interaction. By properly controlling the laser energy density and pulse number (controlled by scanning speed), the conversion between microconvex structure and microconcave structure can be effectively realized. Therefore, as the scanning speed changes from 20 mm/s to 80 mm/s in this work, the number of laser pulses per irradiation points constantly decreases. When the pulse number is relatively high, surface tension dominates the molten pool formed during the laser ablation of the BMG substrate. Due to the increase in surface temperature, the surface tension coefficient might change from negative to positive after reaching a critical temperature value, resulting in a significant change in the flow behavior of molten material. Accordingly, the molten material would exhibit radially inward flow due to the highest temperature in the center of the molten pool, resulting in the formation of a microconvex structure. On the contrary, when the pulse number is relatively low, the molten material would flow radially outward with recoil pressure as the dominating force, leading to the formation of a microconcave structure [35]. In addition, we utilized a UV nanosecond laser with a wavelength of 355 nm for fabrication of a periodic surface structure on the BMG. Besides precisely controlling the type of surface structure, the use of UV laser also demonstrates the effectiveness of reducing the thermal effect and minimizing the heat-affected zone during laser material processing. More importantly, crystallization of the BMG substrate can be effectively avoided [26,36], which lays a solid foundation for surface functionalization of BMGs.
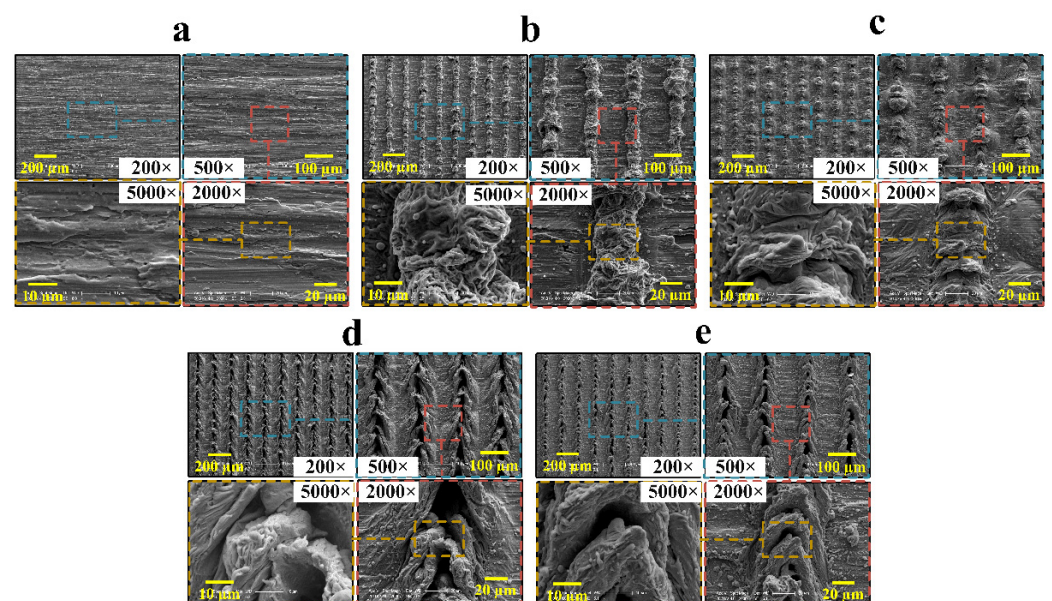

Figure 3. SEM micrographs of untreated BMG surface and laser-structured BMG surfaces at different scanning speeds: (**a**) untreated surface; (**b**) 20 mm/s; (**c**) 40 mm/s; (**d**) 60 mm/s; (**e**) 80 mm/s.

3.2. Surface Chemistry

As discussed by Fasasi et al. [37], the surface chemistry of a metallic substrate can be substantially modified during laser texturing due to material vaporization and laser-induced oxidation. To investigate the evolution of surface chemistry and elemental changes on different BMG surfaces, the XPS elemental analysis technique was employed. Figure 5 and Table 2 show the XPS full spectra and detailed atomic elemental compositions for the untreated BMG surface, the laser-structured BMG surface and the laser-heat-treated BMG surface. As shown in Figure 5a, elements including C, O, Be, Zr, Ti, Ni and Cu

can be detected on the untreated BMG surface. Be, Zr, Ti, Ni and Cu come from the substrate material, whereas O and C originate from the oxidation and slight contamination on the surface layer of the substrate material, respectively. However, after laser surface structuring, the surface chemistry on the laser structured BMG surface exhibits clear changes compared with that of the untreated BMG surface, as shown in Figure 5b. Both of the elements that come from the substrate and the C and O show clear variation of their atomic elemental compositions.
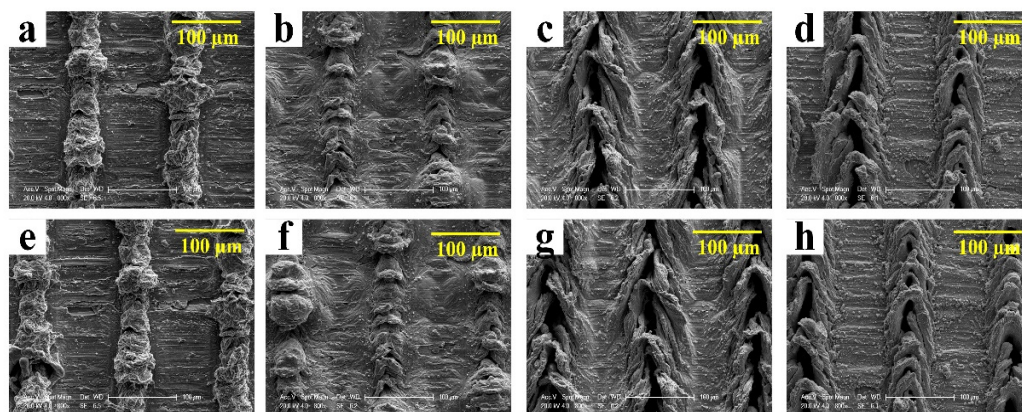

Figure 4. SEM micrographs of laser-structured BMG surfaces at different scanning speeds before and after heat treatment: (**a**) 20 mm/s before heat treatment; (**b**) 40 mm/s before heat treatment; (**c**) 60 mm/s before heat treatment; (**d**) 80 mm/s before heat treatment; (**e**) 20 mm/s after heat treatment; (**f**) 40 mm/s after heat treatment; (**g**) 60 mm/s after heat treatment; (**h**) 80 mm/s after heat treatment.
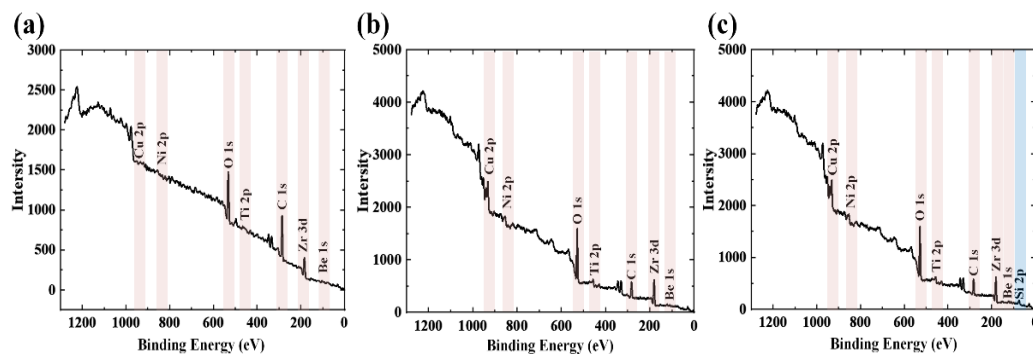

Figure 5. XPS full spectra of (**a**) untreated BMG surface; (**b**) laser-structured BMG surface; (**c**) laser-heat-treated BMG surface.

Table 2. Detailed atomic elemental compositions for the XPS full spectra as shown in Figure 5 (**a**) untreated BMG surface; (**b**) laser-structured BMG surface; (**c**) laser-heat-treated BMG surface.

Element (Atomic %)	Untreated	Laser-Structured	Laser-Heat-Treated
C 1s	62.35	30.85	37.80
O 1s	26.88	47.85	41.51
Be 1s	8.17	8.58	8.16
Zr 3d	2.08	3.91	4.16
Ti 2p	0.18	2.72	1.18
Ni 2p	0.23	1.43	1.46
Cu 2p	0.11	4.66	3.96
Si 2p	-	-	1.77

As seen in Table 2, the atomic elemental composition of C is decreased from 62.35% to 30.85%, whereas the atomic elemental composition of O is increased from 26.88% to 47.85% for the laser-structured BMG surface. This indicates that laser surface structuring not only induced periodic surface structures on the BMG surface but also resulted in strong surface oxidation, leading to the generation of a significant amount of polar functional groups, including −OH and −COOH [38]. For the laser-heat-treated BMG surface, its surface chemistry differs from that of the laser-structured surface in the following two aspects (Figure 5c): (1) The atomic elemental composition of C was increased after heat treatment. (2) Si with an atomic percentage of 1.77% was detected on the heat-treated BMG surface. The increase in the elemental composition of C can be mainly attributed to the deposition of airborne non-polar hydrophobic functional groups ($-CH_2-$, $-CH_3$ and C=C) on the surface, which was accelerated by the heat treatment process. The appearance of Si can be attributed to the silicone seal on the furnace used in this work. During heat treatment at a temperature of 150 °C, the silicon atoms are vaporized into air and then deposited onto the BMG surface, forming a silicon-based thin film [39,40]. This helps to clearly elucidate the change in elemental composition of C and Si on the laser-heat-treated BMG surface.

3.3. Surface Wettability

Surface wettability transition of the BMG surface after each treatment step was experimentally characterized by WCA measurements; the measurement results can be found in Figure 6. The surface wettability can be categorized into four types and represented by the corresponding ranges of WCA values: hydrophobic (90° < WCA < 150°), hydrophilic (10° < WCA < 90°), superhydrophobic (WCA > 150°) and superhydrophilic (WCA < 10°). The WCA on the untreated BMG surface is 86.4 ± 1.2° (Figure 6a), indicating that the untreated BMG surface is hydrophilic. Due to the metastable state of BMG, the atomic binding on the surface is quite weak; therefore, the atoms in BMG appear to be more active than those in crystals with similar chemical compositions. As a result, the surface energy of BMG is relatively high, leading to hydrophilicity [37]. After laser surface structuring, the WCA is reduced to 0°, as shown in Figure 6b. This is mainly attributed to the fact that laser surface structuring notably increases the surface roughness and converts the droplet from unstable Cassie state to saturated Wenzel state on the laser-induced periodic surface structure immediately upon laser structuring, which renders the surface superhydrophilic [38]. The generation of a large amount of polar functional groups, including −OH and −COOH, further contributes to the increase in surface superhydrophilicity. After a 1 h heat treatment, the WCA of the laser heat-treated BMG surface is increased to 147.2 ± 1.7° (Figure 6c), demonstrating high hydrophobicity. Finally, with a heat treatment of 2 h, the laser-heat-treated BMG surface exhibits distinct superhydrophobicity with a WCA of 153.8 ± 2.2° (Figure 6d). The experimental results indicate that with sufficient heat treatment time, the surface wettability of BMG can be effectively converted from superhydrophilicity to superhydrophobicity. As previously discussed, heat treatment distinctly changes the surface chemistry with deposition of airborne non-polar functional groups and silicon-based thin film onto the surface, which are both known to be hydrophobic [39,40]. The combination of these two factors contributes to the realization of superhydrophobicity on the laser-heat-treated BMG surface.

3.4. Evaluation of Tribological Performance

The tribological performance of the untreated surface and the laser-heat-treated superhydrophobic BMG surface under dry sliding and water lubrication conditions was investigated by the ball-on-disc wear test, and the measurement results for average coefficient of friction (COF) can be found in Figure 7 and Table 3. As shown in Figure 7a,b, the COF curve of the untreated BMG surface is much more unstable than that of the laser-heat-treated superhydrophobic surface. The average COF for the laser-heat-treated superhydrophobic BMG surface is reduced by ~45% compared with that of the untreated surface under dry sliding conditions. This is mainly attributed to the reduction in surface

area due to laser ablation, which alters the actual contact area between the friction ball and the laser-heat-treated superhydrophobic BMG surface, lowering the average COF. In contrast, the average COFs for both surfaces exhibit more explicit distinction under water lubrication conditions. With scanning speeds of 20 mm/s and 60 mm/s, the average COFs for the laser-heat-treated superhydrophobic surfaces are 0.246 and 0.233, respectively, with reduction percentages of 51.2% and 54.0% compared with those of the untreated surface (COF = 0.506) using water as the lubrication medium. This indicates that the average COF of the laser-heat-treated superhydrophobic surface can be significantly reduced by the combined effects of lubrication medium, surface wettability and surface structure, resulting in enhancement of the antifriction performance for BMG.
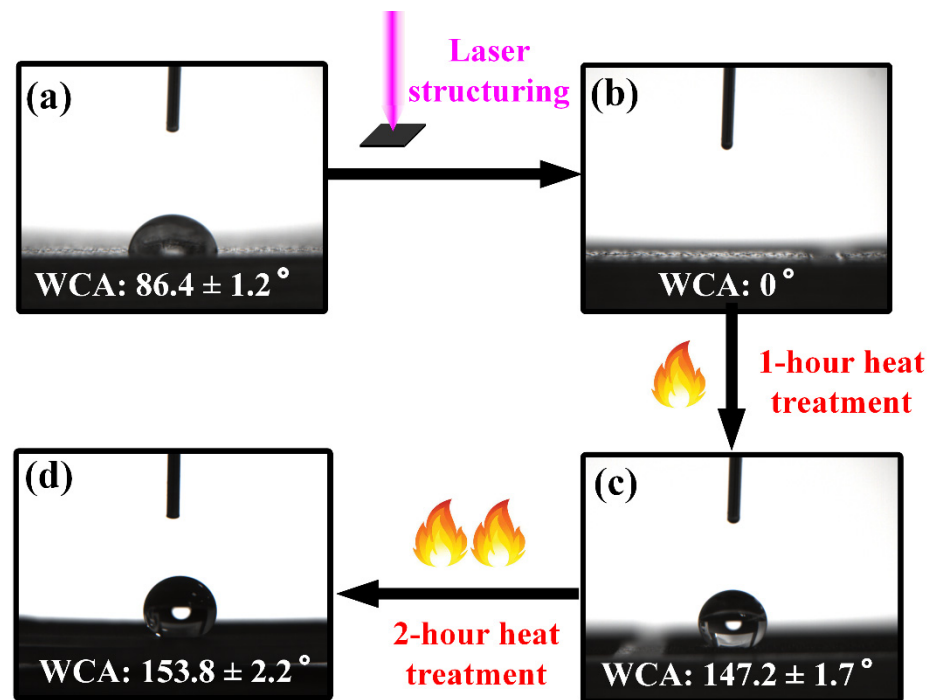

Figure 6. Surface wettability transition of the BMG surface after different treatment steps: (**a**) untreated; (**b**) upon laser structuring; (**c**) 1 h heat treatment after laser structuring; (**d**) 2 h heat treatment after laser structuring.
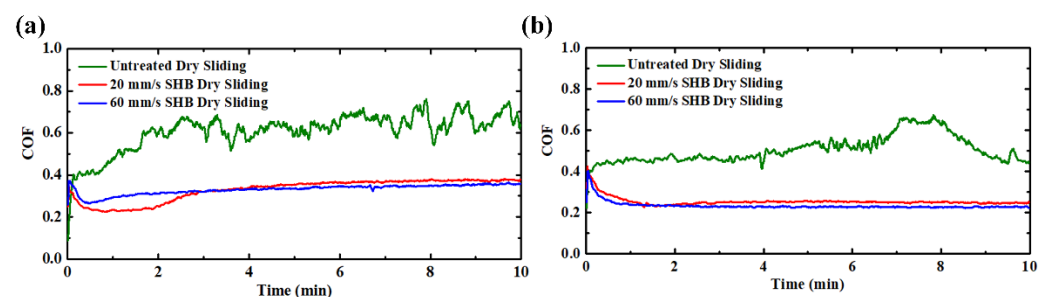

Figure 7. Variations of COF with respect to time for the untreated surface and the laser-heat-treated superhydrophobic (SHB) BMG surface under (**a**) dry sliding and (**b**) water lubrication conditions.

Figure 8 shows the wear morphology of the untreated surface and the laser-heat-treated superhydrophobic BMG surface under different lubrication conditions. As shown in Figure 8a, the wear on the untreated surface is severe under dry sliding conditions, mainly consisting of abrasive wear and a certain amount of adhesion wear. Under water lubrication (Figure 8b), abrasive wear is reduced, and the main wear mode is transformed to adhesion wear. However, distinct wear track can still be observed with high width

and depth. For the laser-heat-treated superhydrophobic BMG surface, slight abrasive wear and adhesion wear can still be observed under dry sliding conditions (Figure 8c), and the antiwear performance is improved relative to the untreated surface. With water lubrication (Figure 8d), a minimum degree of wear can be observed on the laser-heat-treated superhydrophobic BMG surface. On the one hand, abrasive wear totally disappears, and only very slight adhesion wear can be observed. On the other hand, compared with the laser-heat-treated superhydrophobic BMG surface under dry sliding conditions, the width and depth of the wear track is significantly reduced.

Table 3. Average COF for different types of BMG surfaces under dry sliding and water lubrication conditions.

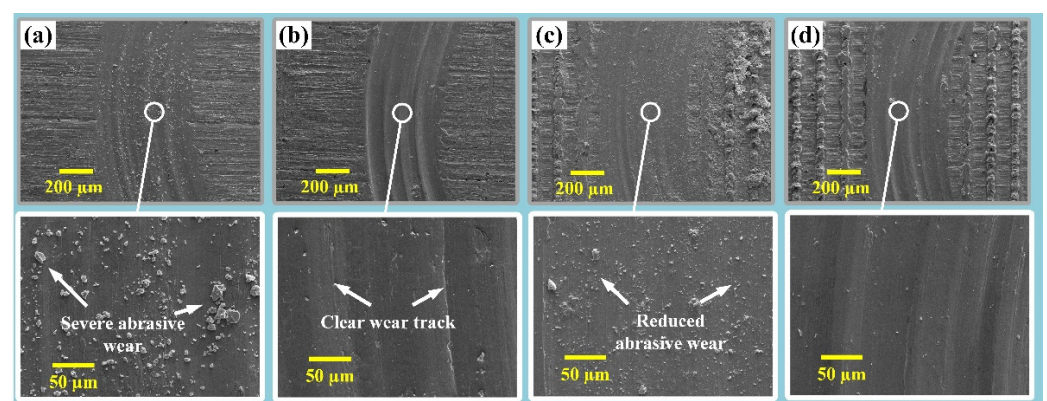| Surface Type	Lubrication Condition	Average COF
Untreated	Dry	0.609
Untreated	Water	0.456
Superhydrophobic + 20 mm/s	Dry	0.330
Superhydrophobic + 20 mm/s	Water	0.246
Superhydrophobic + 60 mm/s	Dry	0.331
Superhydrophobic + 60 mm/s	Water	0.233

Figure 8. SEM images of the worn surfaces under different conditions: (**a**) untreated surface with dry sliding; (**b**) untreated surface with water lubrication; (**c**) laser-heat-treated surface with dry sliding; (**d**) laser-heat-treated surface with water lubrication.

3.5. Processing Mechanism Analysis

In order to understand the experimental observations for surface wettability characterization and wear testing, processing mechanism analyses were conducted for laser-induced surface wettability transition and varied tribological performance under different lubrication conditions. For the surface wettability evolution after different treatment steps, laser surface structuring and subsequent heat treatment should be considered equally important. First, the laser beam interacts with the substrate material, resulting in local heating, melting and vaporization, which induces the generation of a periodic surface structure with either a microconvex structure or a microconcave structure. Then, laser surface structuring alters surface chemistry simultaneously by oxidizing the surface and generating a large amount of hydrophilic functional groups. Finally, heat treatment accelerates the deposition of airborne hydrophobic polar functional groups and induces the generation of hydrophobic silicon-based thin film, resulting in the conversion from superhydrophilicity to superhydrophobicity. Therefore, by properly modulating the surface structure and surface chemistry, the surface wettability evolution can be well controlled. In addition, the underlying wear mechanism for different lubrication conditions is schematically illustrated in Figure 9 and analyzed as follows: (1) Lubrication condition significantly affects the friction characteristics of BMG and can potentially change the wear mode on the surface. This can be mainly attributed the change in contact mode between the friction ball and

surface under different lubrication conditions. Water lubrication can wash away the particles generated during the wear test [41], drastically reducing the extent of abrasive wear. (2) Laser surface structuring can reduce the actual area on the BMG surface by material ablation and vaporization (Figure 9a), which changes the contact area between the friction ball and BMG surface and enhance antifriction performance. (3) With water lubrication, surface wettability considerably affects the tribological performance of the BMG surface. Due to superhydrophobicity, the water film on the laser-heat-treated superhydrophobic BMG surface is relatively thicker during the wear test. It is neither taken away from the area where friction occurs nor squeezed into the grooves by the friction ball. As a result, the lubrication medium can provide persistent protection for the surface layer of the BMG and reduce the depth of wear track and the degree of wear, as shown in Figure 9b. (4) BMG has intrinsic high hardness and good wear resistance [5]. With the combined effects of modified surface structure/surface wettability and proper lubrication conditions, the wear resistance of the BMG surface can be further enhanced. This could provide new insights for fabrication of highly wear-resistant and reliable BMG structural components.
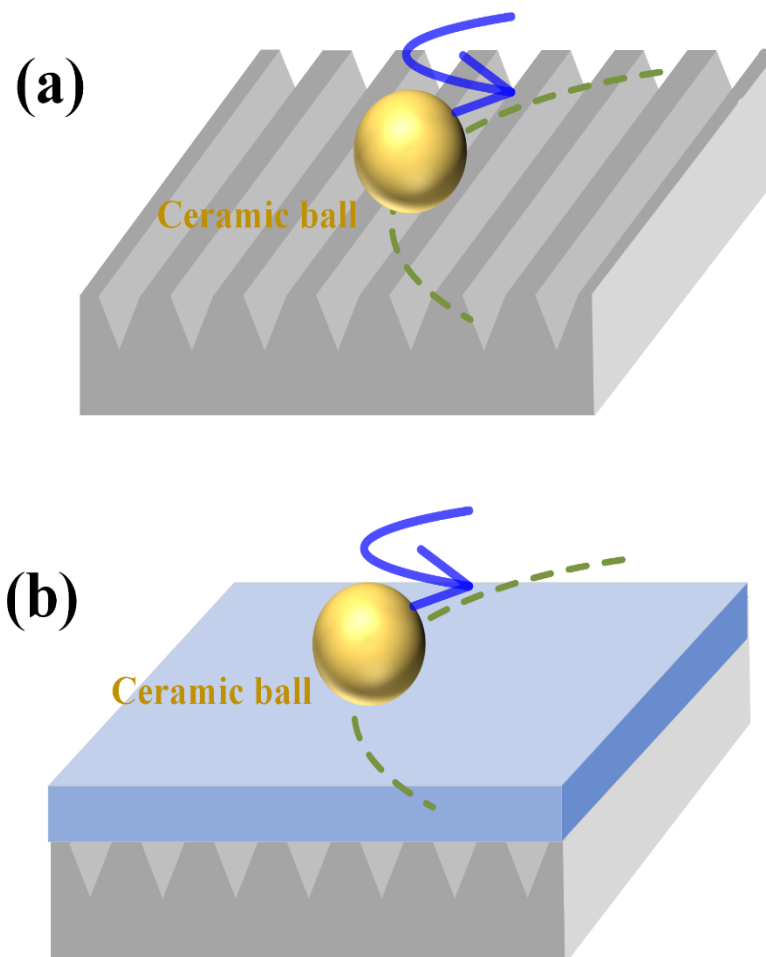

Figure 9. Schematic illustration of wear mechanisms for (**a**) dry sliding and (**b**) water lubrication.

4. Conclusions

In this work, a facile laser-based surface structuring technique was developed to modulate the surface properties, including surface structure, surface chemistry and surface wettability, as well as the tribological performance of Zr-based BMG. The developed two-step laser-based technique was first used to fabricate periodic surface structures, and then heat treatment was employed to alter the surface chemistry/surface energy. The surface wettability of the BMG surface changes from superhydrophilicity immediately upon laser texturing to superhydrophobicity after heat treatment, which can be attributed the com-

bined effects of laser-induced surface structure and surface chemistry. The coefficient of friction was significantly reduced for the laser-heat-treated superhydrophobic surface when water was applied as the lubrication medium, demonstrating the improvement of antifriction performance compared with the untreated surface. This work can be utilized to more efficiently modify the surface properties of BMG, benefiting applications in diverse areas.

Author Contributions: Conceptualization, Q.W. and H.W.; data curation, Q.W., Y.Z., P.W. and C.Q.; formal analysis, Y.Z., P.W. and C.Q.; funding acquisition, Q.W. and H.W.; investigation, Q.W., Y.Z., P.W. and C.Q.; methodology, Q.W.; project administration, Q.W.; resources, Q.W. and H.W.; validation, Q.W.; writing—original draft, Q.W.; writing—review and editing, H.W. All authors have read and agreed to the published version of the manuscript.

Institutional Review Board Statement: Not applicable.

Informed Consent Statement: Not applicable.

Data Availability Statement: Not applicable.

Conflicts of Interest: The authors declare no conflict of interest.

References

1. Chen, M. A brief overview of bulk metallic glasses. *NPG Asia Mater.* **2011**, *3*, 82–90. [CrossRef]
2. Kumar, G.; Desai, A.; Schroers, J. Bulk metallic glass: The smaller the better. *Adv. Mater.* **2011**, *23*, 461–476. [CrossRef]
3. Löffler, J.F. Bulk metallic glasses. *Intermetallics* **2003**, *11*, 529–540. [CrossRef]
4. Telford, M. The case for bulk metallic glass. *Mater. Today* **2004**, *7*, 36–43. [CrossRef]
5. Huang, H.; Yan, J. Investigating shear band interaction in metallic glasses by adjacent nanoindentation. *Mater. Sci. Eng. A* **2017**, *A704*, 375–385. [CrossRef]
6. Li, H.F.; Zheng, Y.F. Recent advances in bulk metallic glasses for biomedical applications. *Acta Biomater.* **2016**, *36*, 1–20. [CrossRef]
7. Khan, M.M.; Nemati, A.; Rahman, Z.U.; Shah, U.H.; Asgar, H.; Haider, W. Recent Advancements in Bulk Metallic Glasses and Their Applications: A Review. *Crit. Rev. Solid State Mater. Sci.* **2018**, *43*, 233–268. [CrossRef]
8. Hirano, T.; Kato, H.; Matsuo, A.; Kawamura, Y.; Inoue, A. Synthesis and mechanical properties of Zr55Al10Ni5Cu30 bulk glass composites containing ZrC particles formed by the in-situ reaction. *Mater. Trans. JIM* **2000**, *41*, 1454–1459. [CrossRef]
9. Kumar, G.; Tang, H.X.; Schroers, J. Nanomoulding with amorphous metals. *Nature* **2009**, *457*, 868–872. [CrossRef]
10. Hu, Z.; Gorumlu, S.; Aksak, B.; Kumar, G. Patterning of metallic glasses using polymer templates. *Scr. Mater.* **2015**, *108*, 15–18. [CrossRef]
11. He, P.; Li, L.; Wang, F.; Dambon, O.; Klocke, F.; Flores, K.M.; Yi, A.Y. Bulk metallic glass mold for high volume fabrication of micro optics. *Microsyst. Technol.* **2016**, *22*, 617–623. [CrossRef]
12. Chen, N.; Frank, R.; Asao, N.; Louzguine-Luzgin, D.V.; Sharma, P.; Wang, J.Q.; Xie, G.Q.; Ishikawa, Y.; Hatakeyama, N.; Lin, Y.C.; et al. Formation and properties of Au-based nanograined metallic glasses. *Acta Mater.* **2011**, *59*, 6433–6440. [CrossRef]
13. Ketov, S.V.; Shi, X.; Xie, G.; Kumashiro, R.; Churyumov, A.Y.; Bazlov, A.I.; Chen, N.; Ishikawa, Y.; Asao, N.; Wu, H.; et al. Nanostructured Zr-Pd metallic glass thin film for biochemical applications. *Sci. Rep.* **2015**, *5*, 7799. [CrossRef]
14. Zhao, M.; Abe, K.; Yamaura, S.; Yamamoto, Y.; Asao, N. Fabrication of Pd−Ni−P Metallic Glass Nanoparticles and Their Application as Highly Durable Catalysts in Methanol Electro-oxidation. *Chem. Mater.* **2014**, *26*, 1056–1061. [CrossRef]
15. Bakkal, M.; Shih, A.J.; Scattergood, R.O.; Liu, C.T. Machining of a Zr-Ti-Al-Cu-Ni metallic glass. *Scr. Mater.* **2004**, *50*, 583–588. [CrossRef]
16. Zhang, X.; Zhang, Y.; Tong, H.; Li, Y.; Chen, X.; Chen, G. Micro-electro-discharge machining of bulk metallic glasses. In Proceedings of the International Symposium on High Density Packaging and Microsystem Integration 2007, HDP'07, Shanghai, China, 26–28 June 2007; pp. 30–33.
17. Wang, H.; Zhuang, J.; Qi, H.; Yu, J.; Guo, Z.; Ma, Y. Laser-chemical treated superhydrophobic surface as a barrier to marine atmospheric corrosion. *Surf. Coat. Technol.* **2020**, *401*, 126255. [CrossRef]
18. Wang, H.; Zhuang, J.; Yu, J.; Qi, H.; Ma, Y.; Wang, H.; Guo, Z. Fabrication of Anti-Reflective Surface with Superhydrophobicity/High Oleophobicity and Enhanced Mechanical Durability via Nanosecond Laser Surface Texturing. *Materials* **2020**, *13*, 5691. [CrossRef]
19. Kedia, S.; Bonagani, S.K.; Majumdar, A.G.; Kain, V.; Subramanian, M.; Maiti, N.; Nilaya, J.P. Nanosecond laser surface texturing of type 316L stainless steel for contact guidance of bone cells and superior corrosion resistance. *Colloid Interface Sci. Commun.* **2021**, *42*, 100419. [CrossRef]

20. Emelyanenko, K.A.; Sanzharovsky, N.A.; Chulkova, E.V.; Ganne, A.A.; Emelyanenko, A.M.; Boinovich, L.B. Superhydrophobic corrosion resistant coatings for copper via IR nanosecond laser processing. *Mater. Res. Express* **2018**, *5*, 115001. [CrossRef]

21. Huang, J.; Guan, Y.; Ramakrishna, S. Tribological behavior of femtosecond laser-textured leaded brass. *Tribol. Int.* **2021**, *162*, 107115. [CrossRef]

22. Nagle Travessa, D.; Vilas Boas Guedes, G.; Capella de Oliveira, A.; Regina Cardoso, K.; Roche, V.; Moreira Jorge, A. The effect of surface laser texturing on the corrosion performance of the biocompatible β-Ti12Mo6Zr2Fe alloy. *Surf. Coat. Technol.* **2021**, *405*, 126628. [CrossRef]

23. Hu, T.; Hu, L.; Ding, Q. The effect of laser surface texturing on the tribological behavior of Ti-6Al-4V. *Proc. Inst. Mech. Eng. Part J J. Eng. Tribol.* **2012**, *226*, 854–863. [CrossRef]

24. Ahuir-Torres, J.I.; Arenas, M.A.; Perrie, W.; Dearden, G.; de Damborenea, J. Surface texturing of aluminium alloy AA2024-T3 by picosecond laser: Effect on wettability and corrosion properties. *Surf. Coat. Technol.* **2017**, *321*, 279–291. [CrossRef]

25. Hu, T.; Hu, L. The study of tribological properties of laser-textured surface of 2024 aluminium alloy under boundary lubrication. *Lubr. Sci.* **2012**, *24*, 84–93. [CrossRef]

26. Huang, H.; Jun, N.; Jiang, M.; Ryoko, M.; Yan, J. Nanosecond pulsed laser irradiation induced hierarchical micro/nanostructures on Zr-based metallic glass substrate. *Mater. Des.* **2016**, *109*, 153–161. [CrossRef]

27. Jiao, Y.; Brousseau, E.; Han, Q.; Zhu, H.; Bigot, S. Investigations in nanosecond laser micromachining on the Zr52.8Cu17.6Ni14.8Al9.9Ti4.9 bulk metallic glass: Experimental and theoretical study. *J. Mater. Process. Technol.* **2019**, *273*, 116232. [CrossRef]

28. Jiao, Y.; Brousseau, E.; Shen, X.; Wang, X.; Han, Q.; Zhu, H.; Bigot, S.; He, W. Investigations in the fabrication of surface patterns for wettability modification on a Zr-based bulk metallic glass by nanosecond laser surface texturing. *J. Mater. Process. Technol.* **2020**, *283*, 116714. [CrossRef]

29. Jiao, Y.; Brousseau, E.; Nishio Ayre, W.; Gait-Carr, E.; Shen, X.; Wang, X.; Bigot, S.; Zhu, H.; He, W. In vitro cytocompatibility of a Zr-based metallic glass modified by laser surface texturing for potential implant applications. *Appl. Surf. Sci.* **2021**, *547*, 149194. [CrossRef]

30. Du, C.; Wang, C.; Zhang, T.; Yi, X.; Liang, J.; Wang, H. Reduced bacterial adhesion on zirconium-based bulk metallic glasses by femtosecond laser nanostructuring. *Proc. Inst. Mech. Eng. Part H J. Eng. Med.* **2020**, *234*, 387–397. [CrossRef]

31. Sawyer, V.; Tao, X.; Dong, H.; Dashtbozorg, B.; Li, X.; Sammons, R.; Dong, H.S. Improving the tribological properties and biocompatibility of Zr-based bulk metallic glass for potential biomedical applications. *Materials* **2020**, *13*, 1960. [CrossRef]

32. Wu, H.; Baker, I.; Liu, Y.; Wu, X.; Munroe, P.R. Effects of environment on the sliding tribological behaviors of Zr-based bulk metallic glass. *Intermetallics* **2012**, *25*, 115–125. [CrossRef]

33. Wu, H.; Liang, L.; Lan, X.; Yin, Y.; Song, M.; Li, R.; Liu, Y.; Yang, H.; Liu, L.; Cai, A.; et al. Tribological and biological behaviors of laser cladded Ti-based metallic glass composite coatings. *Appl. Surf. Sci.* **2020**, *507*, 145104. [CrossRef]

34. Lan, X.; Wu, H.; Liu, Y.; Zhang, W.; Li, R.; Chen, S.; Zai, X.; Hu, T. Microstructures and tribological properties of laser cladded Ti-based metallic glass composite coatings. *Mater. Charact.* **2016**, *120*, 82–89. [CrossRef]

35. Qian, Y.; Jiang, M.; Zhang, Z.; Huang, H.; Yan, J. On the transformation between micro-concave and micro-convex in nanosecond laser ablation of a Zr-based metallic glass. *J. Manuf. Process.* **2021**, *68*, 1114–1122. [CrossRef]

36. Zhang, H.; Qian, Y.; Zhang, L.; Zhang, D.; Liu, H.; Huang, H. Surface coloration of Zr-based metallic glass by nanosecond pulsed laser irradiation in ambient atmosphere. *Mater. Lett.* **2021**, *304*, 130721. [CrossRef]

37. Li, Z.; Ma, J. Water-repellent surfaces of metallic glasses: Fabrication and application. *Mater. Today Adv.* **2021**, *12*, 100164. [CrossRef]

38. Gregorčič, P.; Šetina-Batič, B.; Hočevar, M.; Šetina-Batič, B.; Hočevar, M.; Šetina-Batič, B.; Hočevar, M. Controlling the stainless steel surface wettability by nanosecond direct laser texturing at high fluences. *Appl. Phys. A Mater. Sci. Process.* **2017**, *123*, 766. [CrossRef]

39. Ngo, C.V.; Chun, D.M. Effect of Heat Treatment Temperature on the Wettability Transition from Hydrophilic to Superhydrophobic on Laser-Ablated Metallic Surfaces. *Adv. Eng. Mater.* **2018**, *20*, 1701086. [CrossRef]

40. Wang, Q.; Wang, H.; Zhu, Z.; Xiang, N.; Wang, Z.; Sun, G. Switchable wettability control of titanium via facile nanosecond laser-based surface texturing. *Surf. Interfaces* **2021**, *24*, 101122. [CrossRef]

41. Borruto, A.; Crivellone, G.; Marani, F. Influence of surface wettability on friction and wear tests. *Wear* **1998**, *222*, 57–65. [CrossRef]